PCCP

Excess Electrons Bound to H₂S Trimer and Tetramer Clusters

Complete List of Authors:	Liu, Gaoxiang; The Johns Hopkins University, Department of Chemistry Diaz-Tinoco, Manuel; Auburn University, Department of Chemistry and Biochemistry Ciborowski, Sandra; The Johns Hopkins University, Department of Chemistry Martinez-Martinez, Chalynette; The Johns Hopkins University, Department of Chemistry Lyapustina, Svetlana; The Johns Hopkins University, Department of Chemistry Hendricks, Jay; NIST, Ortiz, Joseph; Auburn University, Department of Chemistry and Biochemistry Bowen, K.; John Hopkins University, Chemistry

SCHOLARONE™
Manuscripts

Excess Electrons Bound to H_2S Trimer and Tetramer Clusters

Gaoxiang Liu[1], Manuel Díaz-Tinoco[2,3], Sandra M. Ciborowski[1], Chalynette Martinez-Martinez[1,4],

Svetlana Lyapustina[1,5], Jay H. Hendricks[1,6], Joseph Vincent Ortiz[2*], Kit H. Bowen[1*]

Addresses:

[1]Department of Chemistry, Johns Hopkins University, Baltimore, MD 21218, USA

[2]Department of Chemistry and Biochemistry, Auburn University, Auburn, AL 36849, USA

Corresponding authors:

* J.V.O.: jvo0001@auburn.edu

* K.H.B: kbowen@jhu.edu

[3]Current address: Department of Physical and Environmental Sciences, University of Toronto

Scarborough, Toronto, Ontario M1C 1A4, Canada and Chemical Physics Theory Group,

Department of Chemistry, University of Toronto, Toronto, Ontario, M5S 3H6, Canada.

[4]Current address: St. Johns River Water Management District, St. Palatka, FL, 32177, USA

[5]Current address: Consortia Management Group, DBR, Washington, DC, 20005, USA

[6]Current address: National Institute of Standards and Technology, Gaithersburg, MD 20899, USA

Abstract

We have prepared the hydrogen sulfide trimer and tetramer anions, $(H_2S)_3^-$ and $(H_2S)_4^-$, measured their anion photoelectron spectra, and applied high-level quantum chemical calculations to interpret the results. The sharp peaks at low electron binding energies in their photoelectron spectra and their diffuse Dyson orbitals are evidence for them both being dipole-bound anions. While the dipole moments of the neutral $(H_2S)_3$ and $(H_2S)_4$ clusters are small, the excess electron induces structural distortions that enhance the charge-dipolar attraction and facilitate the binding of diffuse electrons.

Introduction

Solvated electrons, the simplest quantum solutes, are fundamental species in many fields of physical science.[1-4] In condensed phases, numerous studies have been conducted on the hydrated electron,[5] and to a lesser extent, on solvated electrons in ammonia[6], carbon dioxide[7], alcohols[8], and acetonitrile[9]. In the gas phase, anionic cluster studies have provided molecular-level insight into the solvation environment experienced by excess electrons in the condensed phase.[10-12] These studies have dealt with excess electrons in water clusters[13-22] as well as in clusters of other polar or nonpolar molecules such as NH_3,[23] HF,[24] acetonitrile,[25] methanol,[26] amides,[27] and aromatics.[28]

Hydrogen sulfide (H_2S) is structurally similar to H_2O and possesses the same number of valence electrons. Moreover, the electronegative atoms in both molecules belong to the same group of the periodic table. Differences in their physical properties are primarily due to their differing polarities. The dipole moment of H_2S (0.97 D) is significantly smaller than that of H_2O (1.85 D). Both dipole-dipole and hydrogen bonding interactions between H_2S molecules are extremely weak,[29] whereas these interactions between H_2O molecules are quite strong. The similarities and dissimilarities between them invite comparisons.

Consider for example the observed size distributions of water versus hydrogen sulfide cluster anions, i.e., $(H_2O)_n^-$ vs. $(H_2S)_n^-$, as well as the nature and strength of their excess electron binding. The observed size distribution of $(H_2O)_n^-$ is dominated by n = 2, 6, 7, and starting from 11 continuously on up in size. Based largely on anion photoelectron spectra, the binding of excess electrons to small water clusters is generally thought to be due to dipole binding.[13-18] As we will see below, the observed size distribution of $(H_2S)_n^-$ is limited to n = 3 and 4, almost the opposite to the size distribution of $(H_2O)_n^-$, where the intensities of n = 3 and 4 are typically very weak. The attachment of electrons to larger hydrogen sulfide clusters results in dissociative electron attachment and thus to the observation of $S^-(H_2S)_n$ and $HS^-(H_2S)_n$ cluster anions. The formation of intact $(H_2S)_n^-$ cluster anions appears to be the exclusive province of n = 3 and 4. However, just as in the case of the smallest water cluster anions, e.g., n = 2, our anion photoelectron spectra have revealed spectroscopic signatures of dipole-bound electrons in $(H_2S)_3^-$ and $(H_2S)_4^-$. Furthermore,

our *ab initio* calculations have reproduced the experimentally-determined vertical detachment energies (VDE) values for both $(H_2S)_3^-$ and $(H_2S)_4^-$. However, unlike the cases of the smallest water cluster anions, our experimental and theoretical work when taken together implies a different, more indirect pathway for dipolar excess electron binding in hydrogen sulfide clusters. While there are exceptions, in most cases of dipolar excess electron binding, the structures of the dipole bound anion and its neutral counterpart are very similar, i.e., the excess electron has been attracted to and bound to the dipolar field provided by the largely structurally unperturbed neutral molecule or cluster. In the present cases, however, we found the interaction of excess electrons with hydrogen sulfide trimers and tetramers was able to alter the structures (and polarities) of these neutral clusters to the point where they were able to attach excess electrons though dipole binding. Recently, we have also seen analogous behavior in silatrane molecular anions where internal structural distortions gave rise to dipole binding of excess electrons.[30]

Methods

Experimental

Anion photoelectron spectroscopy (aPES) is conducted by crossing a beam of mass-selected negative ions with a fixed-frequency photon beam and energy-analyzing the resultant photodetached electrons. This technique is governed by the energy-conserving relationship, $hv = EBE + EKE$, where hv is the photon energy, EBE is the electron binding energy, and EKE is the electron kinetic energy. In this work, we have employed two different apparatus both to make hydrogen sulfide cluster anions and to measure their negative ion photoelectron spectra. In one, we used Rydberg electron transfer (RET) to make hydrogen sulfide cluster anions and velocity-map imaging (VMI) to analyze the energies of their photodetached electrons. In the other, employed a nozzle-ion source to prepare hydrogen sulfide cluster anions and a hemispherical deflector to analyze the energies of their photodetached electrons.

Rydberg electron transfer (RET) facilitates formation of diffuse and otherwise weakly bound electron states. In RET, an electronically-excited Rydberg atom transfers its weakly-held, outer

electron to a target neutral molecule or cluster during their collision, resulting in an ion pair which then separates into atomic cation and cluster anion products. RET is a nearly zero electron energy attachment process in which the receding positive ion plays a uniquely stabilizing role. As a result, Rydberg electron transfer provides an unusually gentle, highly quantum state-specific, laser-tunable, anion formation environment. In a RET experiment, atoms are optically pumped to specific Rydberg states (n^*) at the point where they collide with a beam of neutral target molecules or clusters. In the present case, the target is a beam of neutral H_2S clusters formed by the supersonic expansion of a 5% H_2S/He gas mixture from a pulse valve. To generate high intensities of product anions, we used alkali (K) atoms and two pulsed dye lasers. One laser optically pumps potassium atoms to their $^2P_{3/2}$ level, while the second laser selectively excites that population to the *ns* and *nd* Rydberg levels of interest. Several Rydberg levels, i.e., n^*= *12d-15d*, were surveyed, with the most intense ion signal occurring at the n^* = *14d* Rydberg level. The crossing point for beams of Rydberg-excited K atoms and neutral target molecules or clusters is between the ion extraction grids of our time-of-flight mass analyzer/selector. There, hydrogen sulfide cluster anions were formed by RET and accelerated into a flight tube, along which they are mass-selected, prior to being photodetached. The only intact hydrogen sulfide cluster anions observed were $(H_2S)_3^-$ and $(H_2S)_4^-$.

The electron energies of the photodetached electrons were measured using the velocity-map imaging (VMI) technique. There, mass-selected anions were crossed with 1064 nm linearly polarized photons from a Nd:YAG laser. The resultant photodetached electrons were then accelerated along the axis of the ion beam toward a position-sensitive detector, which was coupled to a CCD camera. The basis set expansion (BASEX)[31] Abel transform method was used to reconstruct the two-dimensional image, formed by the sum of these electrons, into a three-dimensional distribution. The resulting anion photoelectron spectra were calibrated relative to the well-known photoelectron spectrum of NO^-. The combination of RET for anion preparation and velocity-map imaging for electron energy analysis on the same apparatus (RET-aPES) is unique and constitutes a sub-category of anion photoelectron spectroscopy. [32-34]

The other apparatus that we used to make hydrogen sulfide cluster anions and measure their negative ion photoelectron spectra employed a nozzle-ion source and a hemispherical electron energy analyzer.[35] The nozzle-ion source produced hydrogen sulfide cluster anions by expanding a mixture of H_2S and argon through a small orifice into high vacuum, where relatively low energy electrons from a nearby biased, hot filament attached to species issuing out the nozzle. The micro-plasma is front of the nozzle was maintained with the help of a weak magnetic field. After ion extraction and transport, mass analysis revealed $(H_2S)_4^-$ to be the only intact hydrogen sulfide cluster anion observed. A mass-selected beam of $(H_2S)_4^-$ was then photodetached with 488 nm photons from an argon ion laser (operated intra-cavity) after which the resulting electrons were energy-analyzed by a hemispherical deflector to provide an anion photoelectron spectrum. Note that while the RET-aPES approach utilized pulsed ion techniques at almost every juncture, the more conventional nozzle-ion/aPES methodology operated in a continuous ion beam fashion at every stage.

Computational

Geometry optimizations on $(H_2S)_3^-$ and $(H_2S)_4^-$ were executed with the coupled-cluster, single, doubles and perturbative triples, or CCSD(T), methods[36] and the doubly-augmented 6-311+^{2}+^{2}G(2df,p) basis-set.[37-39] Exponents of the doubly-augmented basis were obtained by multiplying the most diffuse exponent of each angular momentum from the initial basis set, 6-311++G(2df,p), by 0.3. The abundance of diffuse functions requires that the accuracy criterion of two-electron repulsion integrals be set to 10^{-20} a.u.[40] BD-T1[41-44] electron-propagator calculations of vertical detachment energies (VDE) were performed with augmented, correlation-consistent (aug-cc-pVDZ or aug-cc-pVTZ) basis sets.[45-47] Double, triple and quadruple augmentation of the basis sets (aug^2, aug^3 and aug^4, respectively) was defined by exponents obtained by successively multiplying the most diffuse exponent of each angular momentum by 0.3. VDE values also were inferred from total energy differences at the ΔCCSD(T) level. All electron-propagator pole strengths were above 0.85. Dyson orbitals, expressed as a linear combination of approximate Brueckner orbitals in BD-T1 calculations, were dominated by

a single, pseudo-canonical orbital in every case. These calculations employ the frozen core option. All calculations were performed with Gaussian 16[48], except for the BD-T1 electron-propagator calculations, which employed GDV.[49] Plots of molecular structures and Dyson orbitals were generated with GaussView.[50]

Results and Discussion

The mass spectrum of H_2S trimer and tetramer cluster anions generated by RET is presented in the bottom panel of Figure 1, below the simulated isotope patterns of $S^-(H_2S)_{2,3}$ and $(H_2S)_{3,4}^-$ in the top panels. The peaks at 100 and 134 amu imply the presence of $S^-(H_2S)_2$ and $S^-(H_2S)_3$, in which S^- comes from the dissociative electron attachment of H_2S. The peaks at 104 and 138 amu confirm the formation of $(H_2S)_3^-$ and $(H_2S)_4^-$, as only $(H_2S)_3^-$ and $(H_2S)_4^-$ have isotopes respectively at these two masses. The two mass peaks in the middle, i.e., at 102 and 136 amu, are mixed peaks of $S^-(H_2S)_2/(H_2S)_3^-$ and $S^-(H_2S)_3/(H_2S)_4^-$, respectively. No anions smaller than 90 amu were observed. At larger mass up to 500 amu, $S^-(H_2S)_n$ are the major products (Figure 2), implying that dissociative electron attachment prevails in larger H_2S clusters. Therefore, under our experimental conditions, an excess electron can be attached only to $(H_2S)_3$ and $(H_2S)_4$. As noted above, this size distribution is radically different from that observed among $(H_2O)_n^-$ clusters anions.[13]

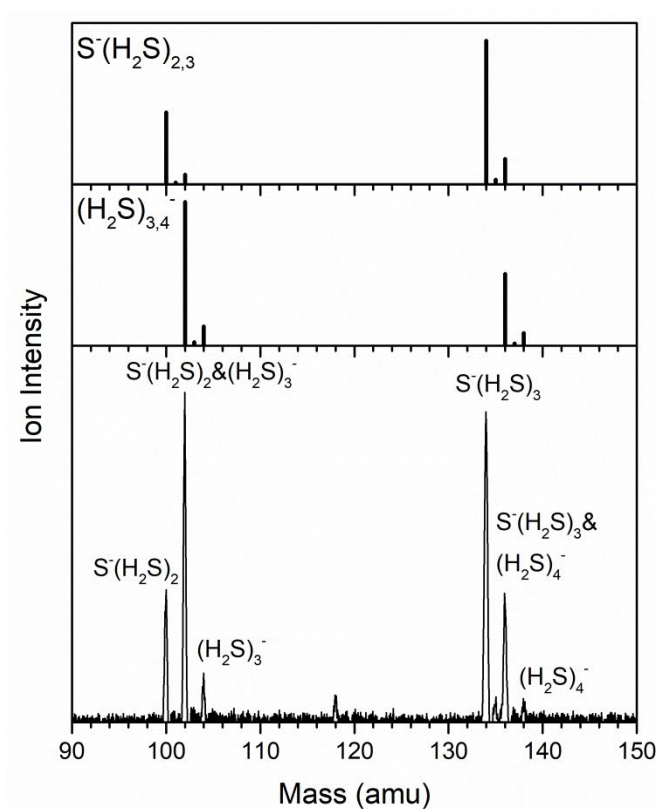**Figure 1.** Simulated isotope patterns of S⁻(H₂S)₂,₃ and (H₂S)₃,₄⁻ (top two panels) and experimental mass spectrum due to Rydberg electron transfer at $n^* = 14d$ (bottom panel).
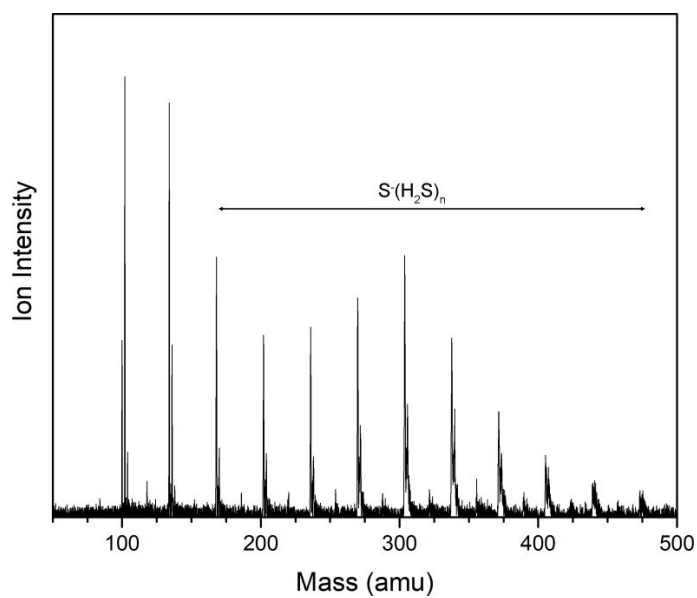

Figure 2. Experimental mass spectrum showing the larger mass anion products made by Rydberg electron transfer at $n^* = 14d$.

Figure 3 presents the anion photoelectron spectra of $(H_2S)_3^-$ and $(H_2S)_4^-$. Spectra on panels (a) and (b) were obtained on the RET-aPES apparatus, while the spectrum presented in (c) was measured with the nozzle-ion source/PES apparatus. Each spectrum consists of a major, sharp peak at low electron binding energy (EBE), strongly implying that $(H_2S)_3^-$ and $(H_2S)_4^-$ are dipole-bound anions. For $(H_2S)_3^-$, the EBE peak is centered at 29 meV, while for $(H_2S)_4^-$, the EBE peak is centered at 115 meV. We assign these two peaks as the origins of the transitions between the cluster anions and their corresponding neutral clusters. Therefore, the vertical detachment energy (VDE) values for $(H_2S)_3^-$ and $(H_2S)_4^-$ are 29 and 115 meV, respectively. In addition to the major peaks, each spectrum also contains a weaker peak on its higher EBE side. These are separated from the center of the strong peak by ~0.34 eV. These peaks are due to the excitation of stretching vibrations (0.33 eV) in the molecular hydrogen sulfide moieties of their clusters.

The photoelectron VMI images embedded in Figure 3 reveals significant anisotropy in both the hydrogen sulfide trimer and tetramer anions. The anisotropy parameters, β, for the photodetached electrons were each estimated to be ~1.7, which approaches the theoretical upper limit. A large β value is consistent with an outgoing p wave, which means that photodetachment occurred from an s-orbital with nearly zero angular momentum. Since both dipole-bound anions have spatially diffuse excess electron states, their excess electrons can be viewed as possessing s-orbital character, consistent with the observed anisotropy.

In complementary experiments on our nozzle-ion source/PES apparatus, we observed $(H_2S)_4^-$ but not $(H_2S)_3^-$. The photoelectron spectrum of $(H_2S)_4^-$ measured on that apparatus is fully consistent with the $(H_2S)_4^-$ spectrum measured on the RET-aPES and in fact exhibits significantly better signal quality. The absence of $(H_2S)_3^-$ in experiments on the nozzle-ion source/PES apparatus is very likely due to its low electron binding energy (29 meV). In the past on that apparatus, we have seen that anions with binding energies below about 40 meV do not make it to the detector, probably because of Stark field detachment. The numerous lenses and deflectors along the ion beam path in that continuous ion beam apparatus present a gauntlet of
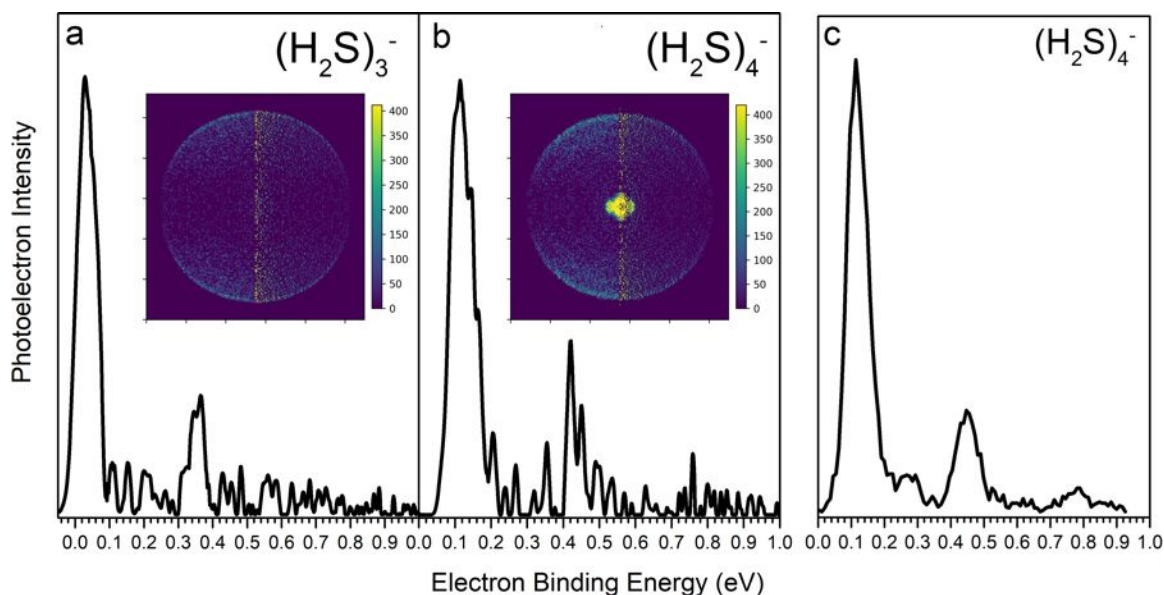
8

Stark-detachment opportunities.

Figure 3 Photoelectron spectra of $(H_2S)_3^-$ and $(H_2S)_4^-$. Spectra in (a) and (b) were obtained on the RET-aPES apparatus with their corresponding photoelectron images embedded in each. The spectrum in panel (c) was measured on the nozzle-ion source/PES apparatus.

The small size of the observed H_2S cluster anions enables the application of high-level *ab initio* calculations to their structures and energetics. Figure 4 presents the optimized structures and the Dyson orbitals of $(H_2S)_3^-$. The two optimized structures have C_{2v} and C_3 symmetry, respectively. Based on the CCSD(T)/aug^3-cc-pVTZ level of theory, the C_{2v} structure is higher in energy than the C_3 structure by 0.048 eV. In the C_{2v} structure, a central H_2S molecule has H bridges to two equivalent H_2S molecules, with all of the H nuclei oriented toward the red contour of the Dyson orbital involved in electron detachment. In the C_3 structure, equivalent sulfur nuclei and three hydrogens form a ring below which lie three hydrogens that are oriented toward the red contour that pertains to the Dyson orbital involved in electron detachment. Both structures of $(H_2S)_3^-$ exhibit positive VDE values only when the basis set is saturated with diffuse basis functions. Triple augmentation suffices for this purpose. After extra diffuse augmentations, there

9

is little difference between results generated with augmented double and triple ζ basis sets. (See Table 1.) BD-T1 results for VDEs are in agreement with ΔCCSD(T) to within a few meV at basis saturation. The predicted VDE values are 21 and 66 meV respectively for the C_3 and C_{2v} structures. The former result, based on the BD-T1 results with quadruple diffuse functions and corresponding to the more stable structure, is in excellent agreement with the observed value, 29 meV.
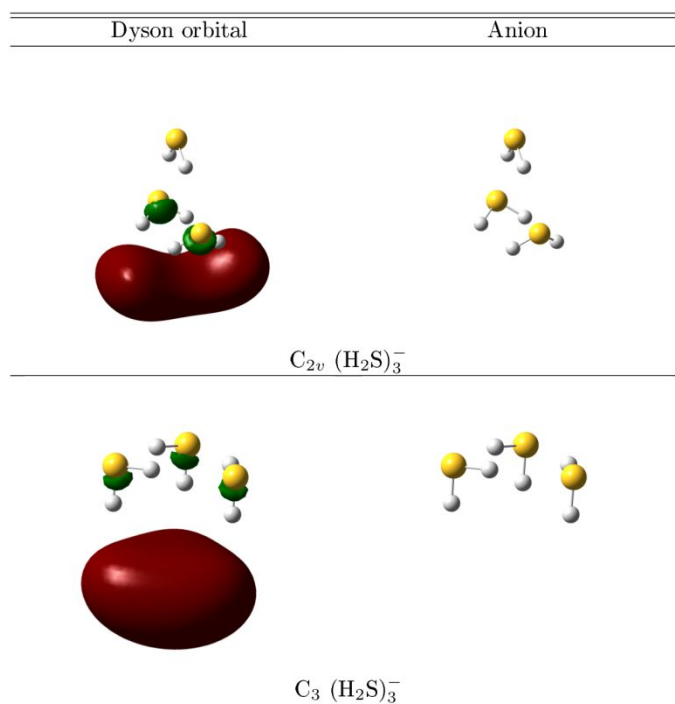

Figure 4. Dyson orbitals and structures for $(H_2S)_3^-$.

Contours of the Dyson orbitals of both isomers indicate that the least bound electron is spread over a volume that lies outside S-H bonds that are oriented to stabilize the extra negative charge. The shapes of the red contours are influenced respectively by the propinquity of three or four H nuclei in the C_3 and C_{2v} structures, respectively. Green contours within S-H bonds indicate orthogonalization to occupied, valence orbitals and delocalization over a larger volume that encloses the molecules in plots of lower contours. The short distance between the majority of the extra negative charge and the nearby H nuclei indicates the importance of electrostatic attraction

in stabilizing the extra negative charge. At such distances, exchange and correlation effects are also important.

Table 1 Calculated vertical detachment energies at different levels of theories for $(H_2S)_3{}^-$.

Expt. VDE	$(H_2S)_3{}^-$		Theo. VDE	
	structure	Basis set	ΔCCSD(T)	BD-T1
0.029	C_3	aug-cc-pVDZ	-0.328	-0.324
		aug^2-cc-pVDZ	-0.040	-0.036
		aug^3-cc-pVDZ	0.011	0.014
		aug^4-cc-pVDZ	0.018	0.021
		aug-cc-pVTZ	-0.243	-0.252
		aug^2-cc-pVTZ	-0.026	-0.029
		aug^3-cc-pVTZ	0.013	0.013
	C_{2v}	aug-cc-pVDZ	-0.211	-0.206
		aug^2-cc-pVDZ	0.027	0.032
		aug^3-cc-pVDZ	0.059	0.064
		aug^4-cc-pVDZ	0.058	0.066
		aug-cc-pVTZ	-0.138	-0.148
		aug^2-cc-pVTZ	0.037	0.034
		aug^3-cc-pVTZ	0.060	0.059

Four optimized structures, labelled by their point groups, are found for $(H_2S)_4{}^-$. The C_4, $C_s{}^1$, $C_s{}^2$ and S_4 (wherein μ=0) clusters are shown in Figure 5. The structures are sensitive to basis sets and to the level of theory; perturbative triples have significant influence on the results. The C_4 structure has the lowest energy at the highest level of theory, ΔCCSD(T)/aug^3-cc-pVTZ, with relative energies for $C_s{}^1$, $C_s{}^2$ and S_4 structures being 0.041, 0.027 and 0.024 eV, respectively. All four anions are bound with respect to neutrals when the basis set is saturated with diffuse

functions (see Table 2). BD-T1 electron-propagator results for VDE values (53, 126, 100 and 25 meV, respectively, for the C_4, C_s^1, C_s^2 and S_4 clusters) are in close agreement with CCSD(T). Results for the two C_s structures are in much closer agreement with the experimental value of 115 meV than those for the more symmetric geometries.
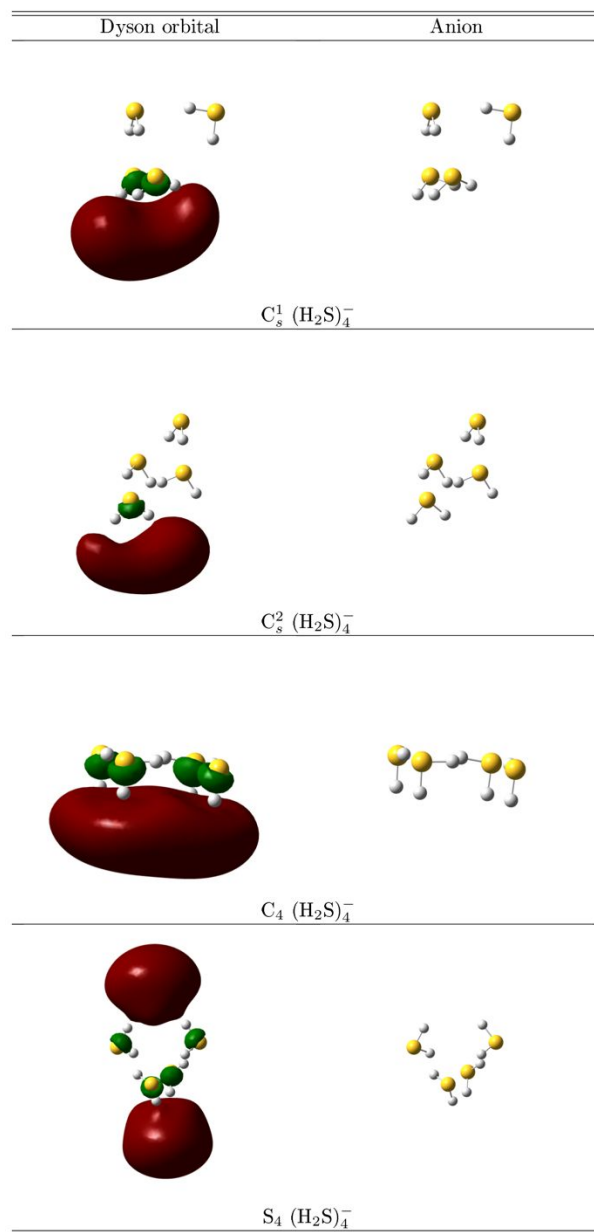

Dyson orbital	Anion

C_s^1 $(H_2S)_4^-$

C_s^2 $(H_2S)_4^-$

C_4 $(H_2S)_4^-$

S_4 $(H_2S)_4^-$

Figure 5. Dyson orbitals and structures of $(H_2S)_4^-$

Table 2. Calculated vertical detachment energies in eV at different levels of theory for $(H_2S)_4^-$.

Expt. VDE	$(H_2S)_4^-$ structure	Basis set	Theo. VDE	
			ΔCCSD(T)	BDT1
0.115	C_4	aug-cc-pVDZ	-0.224	-0.219
		aug^2-cc-pVDZ	0.020	0.024
		aug^3-cc-pVDZ	0.052	0.057
		aug-cc-pVTZ	-0.148	-0.156
		aug^2-cc-pVTZ	0.030	0.028
		aug^3-cc-pVTZ	0.053	0.053
	C_s^1	aug-cc-pVDZ	-0.070	-0.064
		aug^2-cc-pVDZ	0.111	0.117
		aug^3-cc-pVDZ	0.126	0.134
		aug-cc-pVTZ	-0.010	-0.021
		aug^2-cc-pVTZ	0.118	0.113
		aug^3-cc-pVTZ	0.126	0.126
	C_s^2	aug-cc-pVDZ	-0.154	-0.150
		aug^2-cc-pVDZ	0.077	0.082
		aug^3-cc-pVDZ	0.101	0.107
		aug-cc-pVTZ	-0.081	-0.091
		aug^2-cc-pVTZ	0.085	0.082
		aug^3-cc-pVTZ	0.101	0.100
	S_4	aug-cc-pVDZ	-0.238	-0.238
		aug^2-cc-pVDZ	-0.009	-0.008
		aug^3-cc-pVDZ	0.024	0.028
		aug-cc-pVTZ	-0.167	-0.182
		aug^2-cc-pVTZ	0.002	-0.004

	aug^3-cc-pVTZ	0.027	0.025

The latter result can be explained with the aid of Figure 6, which shows that both C_s clusters have an anchoring molecule that binds two, out-of-plane molecules. (Only one of the two latter molecules is visible for C_s^2 in Figure 6; the anchor is at the top right corner in both cases.)   In C_s^1, the anchor also binds an in-plane monomer, but in C_s^2, the two out-of-plane molecules bind it. A path with a low energy barrier between the two minima entails the movement of the monomer on the left of both halves of Figure 6. This fluxionality gives an entropic advantage to the C_s structures over the more ordered C_4 and S_4 alternatives. (An anchor molecule that symmetrically binds two other molecules also is present in the C_{2v} structure of $(H_2S)_3^-$.) The observed VDE value therefore is associated with the fluxional, C_s structures.
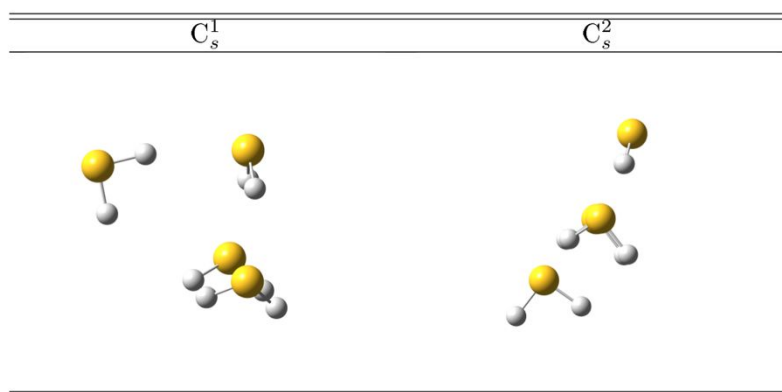

	C_s^1	C_s^2

Figure 6.   Fluctuation between C_s^1 and C_s^2 structures for $(H_2S)_4^-$

Dyson orbitals involved in electron detachment are close to five or six H nuclei, respectively, in the C_s^1 and C_s^2 structures. Volumes enclosed by the corresponding red contours of Figure 6 span regions outside nearby S-H bonds. Orthogonalization to occupied, valence orbitals results in the smaller, green contours and implies delocalization over a larger volume. The C_4 Dyson orbital resembles that of C_3 $(H_2S)_3^-$, but with a higher symmetry axis. A symmetric pattern of delocalization results in the S_4 case.

The dipole moments of the optimized neutral $(H_2S)_3$ and $(H_2S)_4$ clusters, which were calculated in a previous study with MP2/aug-cc-PVTZ[29b] and verified by us in this study with

coupled cluster theory, do not suffice to bind an excess electron. In Table 3, however, we present the dipole moments of the uncharged $(H_2S)_3$ and $(H_2S)_4$ clusters calculated at the geometries of their anions. Under those circumstances, $(H_2S)_4$ would have a large enough dipole moment to electrostatically bind an excess electron. (The practical minimum dipole moment is ~2.5 D.) However, $(H_2S)_3$ would not. Thus, $(H_2S)_3^-$ is probably primarily a correlation-bound excess electron system. In both species, the interactions of their excess electron cause nuclear rearrangements in the clusters that enable binding of diffuse electrons. The short distances between the extra electron's largest amplitudes and the nearest protons indicates the importance of the neutral cluster's electrostatic potential, as well as exchange and electron correlation, in stabilizing the extra negative charge.

Table 3. Calculated dipole moments (Debye) at CCSD/aug^2-cc-pVTZ level of theory for neutral $(H_2S)_3$ and $(H_2S)_4$ at their optimized neutral structures and at their optimized anion structures.

	$\mu_{neutral}{}^{29b}$	Anion geometry	μ_{anion}
$(H_2S)_3$	0.56	C_3	1.93
$(H_2S)_4$	1.39	C_s^1	3.49
		C_s^2	4.37

Summary

We have prepared and characterized the dipole-bound anions of $(H_2S)_3^-$ and $(H_2S)_4^-$. Interactions between an excess electron and a neutral H_2S trimer or tetramer induce structural distortions in the cluster frameworks, which enhance their dipole moments and facilitate the binding of diffuse electrons. In the C_3 structure of $(H_2S)_3^-$, each of the three molecules in a ring with weak, attractive contacts between S lone pairs and a neighboring S-H bond orients its other S-H bond toward a diffuse electron. Two C_s structures of $(H_2S)_4^-$ that are separated by a small barrier also feature re-oriented S-H bonds that stabilize a diffuse electron. While water cluster

anions, $(H_2O)_n^-$, are known to form in a variety of sizes, i.e., n = 2, 6, 7, and from 11 continuously on up, their cousins, hydrogen sulfide cluster anions, $(H_2S)_n^-$, appear to form in only two sizes, n = 3 and 4. Dissimilarities between intermolecular interactions for H_2O versus H_2S are the root cause for observed differences in electron attachment to their clusters.

Acknowledgement

References.

1. E. Alizadeh and L. Sanche, *Chem. Rev.,* 2012, **112**, 5578.

2. F. Arnold, *Nature*, 1981, **294**, 732.

3. J. Gu, J. Leszczynski and H. F. Schaefer III, *Chem. Rev.*, 2012, **112**, 5603.

4. L. Turi and P. J. Rossky, *Chem. Rev.*, 2012, **112**, 5641.

5. (a) E. J. Hart and M. Anbar, *The Hydrated Electron*, (Wiley-Interscience, New York, 1970), (b) J. Savolainen, F. Uhlig, S. Ahmed, P. Hamm and P. Jungwirth, *Nat. Chem.*, 2014, **6**, 697. (c) K. R. Siefermann, Y. Liu, E. Lugovoy, O. Link, M. Faubel, U. Buck, B. Winter and B. Abel *Nat. Chem.*, 2010, **2**, 274. (d) D. Luckhaus, Y. Yamamoto, T. Suzuki and R. Signorell, *Sci. Adv.* 2017, **3**, e1603224. (e) J. M. Herbert and Marc P. Coons, *Annu. Rev. Phys. Chem.*, 2017. **68**, 447.

6. (a) W. Weyl, *Ann. Phys.*, 1864, **199**, 350. (b) J. Lindner, A. N. Unterreiner and P. Vöhringer, *Chem. Phys. Chem.*, 2006, **7**, 363. (c) F. A. Uribe, T. Sawada and A. J. Bard, *Chem. Phys. Lett.*, 1983, **97**, 243. (d) E. Zurek, P. P. Edwards and R. A. Hoffmann, *Angew. Chem., Int. Ed.* 2009, **48**, 8198.

7. Z. Wang, J. Liu, M. Zhang, R. I. Cukier and Y. Bu, *Phys. Rev. Lett.*, 2012, **108**, 207601.

8. (a) C. Silva, P. K. Walhout, P. J. Reid and P. F. Barbara, *J. Phys. Chem. A*, 1998, **102**, 5701. (b) M. J. Tauber, C. M. Stuart and R. A. Mathies, *J. Am. Chem. Soc.*, 2004, **126**, 3414. (c) A. Thaller, R. Laenen and A. Laubereau, *J. Chem. Phys.*, 2006, **124**, 024515. (d) A. T. Shreve, M. H. Elkinsa and D. M. Neumark, *Chem. Sci.*, 2013, **4**, 1633.

9. (a) C. Xia, J. Peon, and B. J. Kohler, *Chem. Phys*. 2002, **117**, 8855. (b) I. A. Shkrob and J. Sauer, *J. Phys. Chem. A*, 2002, **106**, 9120. (c) S. C. Doan and B. J. Schwartz, *J. Phys. Chem. Lett.*, 2013, **4**, 1471.

10. (a) R. E. Larsen, W. J. Glover and B. J. Schwartz, *Science*, 2010, **329**, 65. (b) L. Turi, and A. Madarász, *Science*, 2011, **331**, 1387.

11. R. M. Young and D. M. Neumark, *Chem. Rev.*, 2012, **112**, 5553.

12. A. W. Castleman and K. H. Bowen, *J. Phys. Chem*., 1996, **100**, 12911.

13. J. V. Coe, G. H. Lee, J. G. Eaton, S. T. Arnold, H. W. Sarkas, C. Ludewigt, H. Haberland, D. R. Worsnop and K. H. Bowen, *J. Chem. Phys.*, 1990, **92**, 3980.

14. S. T. Arnold, J. G. Eaton, D. Patel-Misra, H. W. Sarkas, and K. H. Bowen, in *Ion and Cluster ion Spectroscopy and Structure*, edited by J. P. Maier (Elsevier, Amsterdam, 1989), pp. 417-472.

15. N. I. Hammer, J. W. Shin, J. M. Headrick, E. G. Diken, J. R. Roscioli, G. H. Weddle and M. A. Johnson, *Science*, 2004, **306**, 675.

16. T. Sommerfeld and K. D. Jordan, *J. Am. Chem. Soc*., 2006, **128**, 5828.

17. H. M. Lee, S. Lee and K. S. Kim, *J. Chem. Phys.*, 2003, **119**, 187.

18. J. R. R. Verlet, A. E. Bragg, A. Kammrath, O. Cheshnovsky and D. M. Neumark, *Science*, 2005, **307**, 93.

19. L. Turi, W. S. Sheu, P. J. Rossky, *Science,* 2005, **309**, 914.

20. L. A. Posey, P. J. Campagnola, M. A. Johnson, G. H. Lee, J. G. Eaton and K. H. Bowen, *J. Chem. Phys*., 1998, **91**, 6536.

21. H. Haberland and K. H. Bowen, in Clusters of Atoms and Molecules, ed., H. Haberland (Springer-Verlag: Heidelberg, 1993), 134-153.

22. G. H. Lee, S. T. Arnold, J. G. Eaton, H. W. Sarkas, K. H. Bowen, C. Ludewigt and H. Haberland, *Z. Phys. D.*, 1991, **20**, 9.

23. (a) H. W. Sarkas, S. T. Arnold, J. G. Eaton, G. H. Lee and K. H. Bowen, *J. Chem. Phys*., 2002, **116**, 5731. (b) I. R. Lee, W. Lee and A. H. Zewail, *Chem. Phys. Chem*. 2008, **9**, 83. (c) T. Sommerfeld, *J. Phys. Chem. A,* 2008, **112**, 11817.

24. M. Gutowski, C. S. Hall, L. Adamowicz, J. H. Hendricks, H. L. de Clercq, S. A. Lyapustina, J. M. Nilles, S.-J. Xu and K. H. Bowen, *Phys, Rev. Lett.*, 2002, **88**, 143001.

25. (a) T. Takayanagi, T. Hoshino, K. Takahashi, *Chem. Phys.,* 2006, **324**, 679. (b) M. Mitsui,N. Ando, S. Kokubo, A. Nakajima and K. Kaya, *Phys. Rev. Lett.*, 2003, **91**, 153002.

26. A. Kammrath, Jan R. R. Verlet, G. B. Griffin and Daniel M. Neumark, *J. Chem. Phys*., 2006, **125**, 171102.

27. (a)T. Maeyama, K. Yoshida and A. Fujii, *J. Phys. Chem. A*, 2012, **116**, 3771. (b) M. Seydou, A. Modelli, B. Lucas, K. Konate, C. Desfrancois and J.P. Schermann, *Eur. Phys. J. D*, 2005, **35**, 199. (c) T. Maeyama, Y. Negishi, T. Tsukuda, I. Yagia and N. Mikami, *Phys. Chem. Chem. Phys.,* 2006, **8**, 827.

28. M. Mitsui, A. Nakajima and K. J. Kaya, *Chem. Phys.*, 2002, **117**, 9740.

29. (a) A. Das, P. K. Mandal, F. J. Lovas, C. Medcraft, N. R. Walker. E. Arunan, *Angew. Chem. Int. Ed.*, 2018, **57**, 15199. (b) Y. N. Kalugina, D.A. Shuchugashev, V.N. Cherepanov, *Chem. Phys. Lett.*, 2018, **692**, 184.

30. E. F. Belogolova, G. Liu, E. P. Doronina, S. Ciborowski, V. F. Sidorkin and K. H. Bowen, *J. Phys. Chem. Lett*., 2018, **9**, 1284.

31. V. Dribinski, A. Ossadtchi, V. A. Mandelshtam and H. Reisler, *Rev. Sci. Instrum.* 2002, **73**, 2634.

32. (a) S. M. Ciborowski, R. M. Harris, G. Liu, C. J. Martinez-Martinez, P. Skurski, and K. H. Bowen, 2019, *J. Chem. Phys.*, **150,** 161103. (b) S. M. Ciborowski, G. Liu, J. D. Graham, A. M. Buytendyk and K. H. Bowen, *Eur. Phys. J. D*, 2018, **72**, 139.

33. (a) G. Liu, S. M. Ciborowski, J. Graham, A. M. Buytendyk, and K. H. Bowen, *2019, J. Chem. Phys*., **151**, 101101. (b) G. Liu, S. M. Ciborowski, C. R. Pitts, J. D. Graham, A. M. Buytendyk, T. Leckta, and K. H. Bowen, *Phys. Chem. Chem. Phys.*, 2019, **21**, 18310-18315.

34. V. Sidorkin, E. F. Belogolova, E. P. Doronina, G. Liu, S. M. Ciborowski, and K. H. Bowen, J. Am. Chem. Soc, 2020, https://doi.org/10.1021/jacs.9b11694

35. J. H. Hendricks, H. L. De Clercq, C. B. Freidhoff, S. T. Arnold, J. G. Eaton, C. Fancher, S. A.

Lyapustina, J. T. Snodgrass and K. H. Bowen, *J. Chem. Phys.,* 2002, **116**, 7926.

36. K. Raghavachari, G.W. Trucks, J.A. Pople and M. Head-Gordon, *Chem. Phys. Lett.*, 1989, **157**, 479-483.

37. R. Krishnan, J.S. Binkley, R. Seeger and J.A. Pople, *J. Chem. Phys.*, 1980, **72**, 650.

38. T. Clark, J. Chandrasekhar, G.W. Spitznagel and P.v.R. Schleyer, *J. Comput. Chem.*, 1983, **4** 294.

39. A.D. McLean and G.S. Chandler, *J. Chem. Phys.* 1980, **72**, 5639.

40. M. Czapla, J. Simons and P. Skurski, *Phys. Chem. Chem. Phys*, 2018, **20**, 21739.

41. J. V. Ortiz, *Chem. Phys. Lett.*, 1998, **296**, 494.

42. J. V. Ortiz. *Chem. Phys. Lett.*, 1998, **297**, 193.

43. J.V. Ortiz, *Wiley Interdisciplinary Reviews: Computational Molecular Science*, 2013, **3**, 123.

44. J. V. Ortiz, *Annual Reports in Computational Chemistry*, **13**, 139-182, Elsevier, 2017.

45. T. H. Dunning, *J. Chem. Phys.*, 1989, **90**, 1007.

46. R.A. Kendall, T.H. Dunning and R.J. Harrison, *J. Chem. Phys.*, 1992, **96**, 6796.

47. D.E. Woon and T.H. Dunning, *J. Chem. Phys.*, 1993, **98**, 1358.

48. M.J. Frisch, G.W. Trucks, H.B. Schlegel, G.E. Scuseria, M.A. Robb, J.R. Cheeseman, G. Scalmani, V. Barone, G.A. Petersson, H. Nakatsuji, X. Li, M. Caricato, A.V. Marenich, J. Bloino, B.G. Janesko, R. Gomperts, B. Mennucci, H.P. Hratchian, J.V. Ortiz, A.F. Izmaylov, J.L. Sonnenberg, D. Williams-Young, F. Ding, F. Lipparini, F. Egidi, J. Goings, B. Peng, A. Petrone, T. Henderson, D. Ranasinghe, V.G. Zakrzewski, J. Gao, N. Rega, G. Zheng, W. Liang, M. Hada, M. Ehara, K. Toyota, R. Fukuda, J. Hasegawa, M. Ishida, T. Nakajima, Y. Honda, O. Kitao, H. Nakai, T. Vreven, K. Throssell, J. Montgomery, J.A., J.E. Peralta, F. Ogliaro, M.J. Bearpark, J.J. Heyd, E.N. Brothers, K.N. Kudin, V.N. Staroverov, T.A. Keith, R. Kobayashi, J. Normand, K. Raghavachari, A.P. Rendell, J.C. Burant, S.S. Iyengar, J. Tomasi, M. Cossi, J.M. Millam, M. Klene, C. Adamo, R. Cammi, J.W. Ochterski, R.L. Martin, K. Morokuma, O. Farkas, J.B. Foresman and D.J. Fox, Gaussian 16, Gaussian, Inc., Wallingford CT, 2016.

49. M. J. Frisch, G. W. Trucks, H. B. Schlegel, G. E. Scuseria, M. A. Robb, J. R. Cheeseman, G.

Scalmani, V. Barone, G. A. Petersson, H. Nakatsuji, X. Li, M. Caricato, A. V. Marenich, J. Bloino, B. G. Janesko, R. Gomperts, B. Mennucci, H. P. Hratchian, J. V. Ortiz, A. F. Izmaylov, J. L. Sonnenberg, D. Williams-Young, F. Ding, F. Lipparini, F. Egidi, J. Goings, B. Peng, A. Petrone, T. Henderson, D. Ranasinghe, V. G. Zakrzewski, J. Gao, N. Rega, G. Zheng, W. Liang, M. Hada, M. Ehara, K. Toyota, R. Fukuda, J. Hasegawa, M. Ishida, T. Nakajima, Y. Honda, O. Kitao, H. Nakai, T. Vreven, K. Throssell, J. A. Montgomery, Jr., J. E. Peralta, F. Ogliaro, M.J. Bearpark, J. J. Heyd, E. N. Brothers, K. N. Kudin, V. N. Staroverov, T. A. Keith, R. Kobayashi, J. Normand, K. Raghavachari, A. P. Rendell, J. C. Burant, S. S. Iyengar, J. Tomasi, M. Cossi, J. M. Millam, M. Klene, C. Adamo, R. Cammi, J. W. Ochterski, R. L. Martin, K. Morokuma, O. Farkas, J. B. Foresman and D. J. Fox, Gaussian Development Version, Revision I.14+, Gaussian, Inc., Wallingford CT, 2018.

50. R. Dennington, T.A. Keith and J.M. Millam, GaussView, Version 6, Semichem Inc., Shawnee Mission, KS, 2016.